Effects of Processing Route on Morphology and Mechanical Behavior of Polypropylene in Equal Channel Angular Extrusion

Tinglan Wang, Songchao Tang, Jianding Chen

Shanghai Key Laboratory of Advanced Polymeric Materials, Key Laboratory for Ultrafine Materials of Ministry of Education, School of Materials Science and Engineering, East China University of Science and Technology, Shanghai 200237, China

Received 26 July 2010; accepted 28 February 2011
DOI 10.1002/app.34335
Published online 13 June 2011 in Wiley Online Library (wileyonlinelibrary.com).

ABSTRACT: Changes of morphology and mechanical behavior of isotactic polypropylene (iPP) due to equal channel angular extrusion (ECAE) were investigated. The iPP specimens were processed for up to two passes in the same direction (route A), with the specimens rotate 180°around loading axis after the previous pass (route C). The macroscopic observation showed that high level of shear strain is introduced in iPP extruded twice in route A. Reflected optical microscopy revealed that the original spherulites are elongated into ellipsoidal shape along the shear direction in route A, and the recovery of the spherulitic shape occurred in iPP extruded in route C. X-ray diffraction results and the dynamic mechanical analysis showed that the crystalline and amorphous phase are prone to orientation more favorably via route A than route C. The increase of the dynamic storage modulus (E') indicated that iPP becomes stiffer than other samples when extruded twice in route A. Izod impact testing results demonstrated that the ECAE-deformed spherulites influence the crack propagation direction. The impact strength of iPP is greatly improved to 490.5 J/m after processed twice in route A, 10 times of that of undeformed reference sample. © 2011 Wiley Periodicals, Inc. J Appl Polym Sci 122: 2146–2158, 2011

Key words: isotactic polypropylene; equal channel angular extrusion; processing route; orientation

INTRODUCTION

Equal channel angular extrusion (ECAE), an effective metal forming technique developed by Segal in 1981,[1] has abstracted extensive interest in the last few years in manipulating the morphology of polymer in solid state. In contrast to other known solid state polymer processing methods including die drawing,[2] hydrostatic extrusion,[3] plane-strain compression,[4] and rolling,[5] ECAE technique has been identified as an advantageous method for inducing bulk simple shear into polymer. Theoretically, the simple shear strain as high as 200% could be achieved in one pass extrusion.[6] Many polymer systems such as LLDPE,[7] HDPE,[8] PET,[9] PC,[10,11] PMMA,[12] glass fiber/polyacetal composites[13] and clay/nylon-6 nano-composites[14] has been shear deformed by ECAE to achieve molecular or second-phase orientation.

Correspondence to: J. Chen (jiandingchen@ecust.edu.cn).
Contract grant sponsor: Shanghai Leading Academic Discipline Project; contract grant number: B502.
Contract grant sponsor: Shanghai Key Laboratory Project; contract grant number: 08DZ2230500.

Another unique advantage of ECAE is that the specimen has the same cross-sectional area as the original one, which makes different controlled molecular orientation possible by multi-pass extrusion.[15] If the specimen is processed repetitively without any rotation, which is called route A, the total shear strain that the specimen experienced will be progressively accumulated. However, there are some difficulties to achieve multi-pass processing in route A due to the existence of warping[15] of extruded polymer. Therefore, in previous studies most polymer systems were processed for only one pass in route A, except that LLDPE was processed for up to four passes in route A by Sue and Li.[7] The optical microscopy demonstrated that the spherulites of LLDPE are highly deformed and transformed into fibrillar lamellar bundles after four passes extrusion in route A. If the specimen is processed in route C, that is, the specimen is rotated 180°around its loading axis after the previous pass, then the total shear strain will be removed in theory. The result of PET processed for the second pass in route C by Xia et al.[9] confirmed that part of the macrofibrils orientation is eliminated but the local lamellar orientation is still maintained in route C.

The physical and mechanical properties of isotactic polypropylene (iPP) depend strongly upon its

morphology, thus controlled morphology is greatly appreciated in many cases. ECAE was conducted on iPP by Philips et al.,[16] in which highly oriented crystalline lamellae in iPP sample were obtained after two passes extrusion in route A. However, the mechanical properties of iPP so processed were not reported and the structure–property relationship was not elucidated. Furthermore, the effect of route C on the microstructure and the mechanical properties of iPP have not been investigated. In this study, the iPP specimens were processed at 65°C using an experimental ECAE setup. To understand the effect of processing route on iPP, the macroscopic flow behavior and the morphology of iPP specimens processed for up to two passes in routes A and C is studied. Particular attention is paid to analysis the mechanical behavior of iPP sample for understanding the result influence of the morphology changing.

EXPERIMENTAL

Materials

Isotactic polypropylene (T300) was supplied by Shanghai Petrochemical, China (MFI = 3.0 g/10 min, 230°C, 2.16 kg).

Equal channel angular extrusion

ECAE experiments were performed using a die with a 90° intersected angular channel of identical cross section of 13.5 × 13.5 mm^2 [as shown in Fig. 1(a)]. The ECAE die was installed on an electromechanical universal testing machine CMT4204 (SANS, China). The ECAE of iPP was conducted at 65°C and under a constant ram speed of 25 mm/min. The shear deformation occurs when iPP was pushed through the crossing plane of die channels. The load needed for deformation was recorded as a function of the ram displacement for each extrusion. The flow direction (FD), loading direction (LD) and transverse direction (TD) were defined to describe the ECAE process and the measured samples. The iPP specimens were injection molded into 3.3 mm thick, 13.2 mm wide, and 90 mm long bars. Four specimens were coextruded through the ECAE die. One particular advantage of this coextrusion is that a group of specimens are easily split for mechanical tests without cutting or polishing along TD. Two specimens in the middle of four specimens for each procession were selected and machined carefully for dual cantilever mode dynamic mechanical analysis (DMA) and Izod impact testing. The testing directions were also indicated by arrows in Figure 1(a). The extrusions of route A and route C were schematically shown in Figure 1(b).[14] For simplicity, samples before and after ECAE were labeled as follow : (1) reference, (2) A1 sample- extruded in route A, pass one, (3) A2 sample-extruded in route A, pass two, and (4) C2 sample- extruded in route C, pass two.

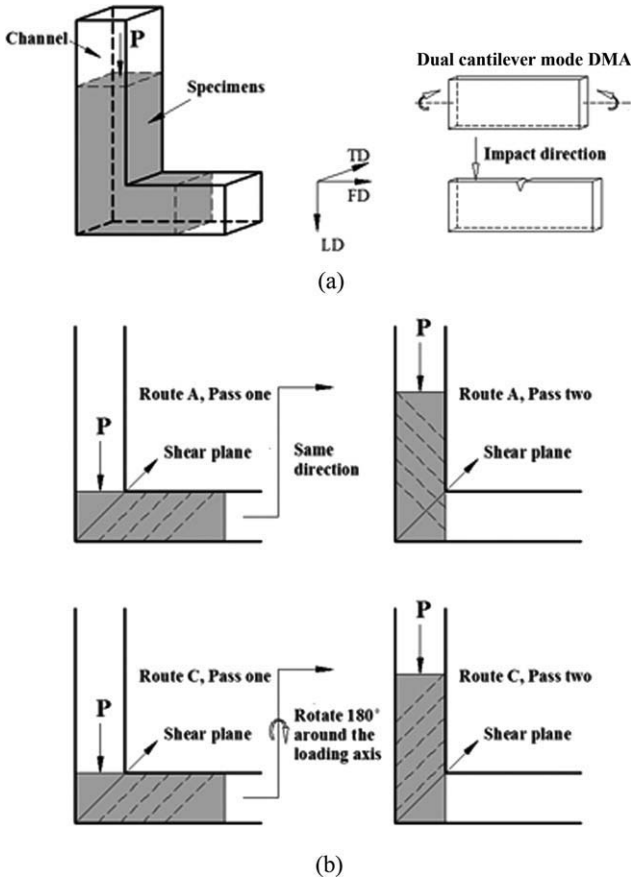

Figure 1 Schematic illustration of ECAE of (a) general process and (b) route A and route C.

Macroscopic observation

The grid lines with a size of 2.0 × 2.0 mm^2 were marked on the FD-LD plane of specimen before extrusion, which can demonstrate the macroscopic deformation of iPP after ECAE.

Reflected optical microscopy

The permanganic etching technique[17] was employed to study the changes in the spherulitic morphology. For etching, the 3 wt % of fine powdered $KMnO_4$ was slowly added under agitation to a 2 : 1 mixture (by volume) of concentrated H_2SO_4 and H_3PO_4. The FD-LD plane of sample was polished carefully to remove the outer surface about 1 mm. Then the samples were floated with the polished surface downward in the etching solution for 12 h at room temperature. After etching, samples were washed in an ultrasound H_2O_2 30% bath. Reflected optical microscopy (ROM) of etched surfaces was taken by a Nikon LV100POL microscope.

Differential scanning calorimetry

The thermal measurement was carried out on Modulated DSC2910 differential scanning calorimeter purged with nitrogen. Each sample was measured in the range of 25–150°C at a heating rate of 10°C/min. The crystallintity X_{DSC} was calculated from the ratio of $\Delta H/\Delta H_o$, where ΔH is the enthalpy of fusion of tested sample, and ΔH for 100% crystalline iPP is taken as 148 J/g.[18]

Density measurement

Density measurement was performed according to ASTM D792. Sample weight in air and in isopropanol (0.785 g/cm^3) was measured at 23°C. The volume degree of crystallinity X_V was calculated by:

$$X_V = \frac{\rho - \rho_g a}{\rho_c - \rho_a} \quad (1)$$

where, ρ_c is the perfect crystalline density (0.936 g/cm^3) and ρ_a is the amorphous density (0.854 g/cm^3).

X-ray characterization

X-ray diffraction was measured by Rigaku D/max 2550 PC diffractometer with Cu-Kα radiation at 40 KV and 300 mA. The X-ray beam was perpendicular to the FD-LD plane of samples. The X-ray diffraction curves were collected during 2θ scan at a speed of 10°/min in the region of 5–50°. The crystallinity X_{XRD} for each sample was obtained from the ratio between the area under the crystalline peaks and the total area under the X -ray diffraction curve. The azimuthal scans of (110), (040), and (130) planes were carried out using a fiber specimen attachment at a scan speed of 72°/min with the azimuthal angle varying from −90° to 270°.

Dynamic mechanical analysis

The dynamic mechanical behavior of samples was obtained by TA 2980 dynamic mechanical analyzer. Penetration mode DMA was performed with of a controlled force of 0.005*N*. The temperature was elevated from 25 to 150°C with a rate of 3°C/min. Dual cantilever mode DMA was measured at a fixed frequency of 1 Hz and a heating rate of 3°C/min. The storage modulus (E') and loss tangent (tan δ) were recorded as a function of temperature ranged from −50 to 150°C.

Optical measurement

The transparency of iPP samples was determined on 3.3 mm thick injection molded plates. The luminous transmittance was measured according to ASTM D 1003 using a spectrophotometer (WGW, China). The size of each tested sample was smaller than the standard size requirement but was large enough to cover the entrance port of the integrating sphere.

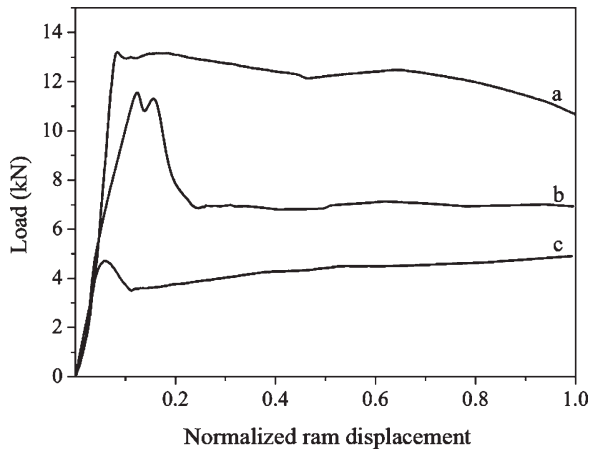

Figure 2 The load as a function of the ram displacement normalized by the length of specimen during the extrusions of (a) route A, pass one, (b) route A, pass two, and (c) route C, pass two.

Izod impact testing and scanning electron microscope

The impact property of the iPP samples was evaluated from notched Izod testing according to ASTM D256. The notch was milled at the top of each sample. The impact fractured surfaces were coated with Au, and then observed by the JSM-6360LV SEM.

RESULTS AND DISCUSSION

Macroscopic deformation behavior of iPP ECAE

The load history that the specimens experienced is helpful to investigate the deformation behavior of iPP during ECAE process. The curves of load versus normalized ram displacement were plotted in Figure 2. The load curve of iPP extruded one pass in route A [Fig. 2(a)] was similar to that of PET.[19] In the primary stage of the extrusion, the load increased rapidly as the specimens were pushed by a ram in the vertical channel of the ECAE die. When the specimens passed through shear plane, the load reached its maximum 13.2 kN. After that, a nearly constant load plateau was followed, which related to the uniform shear deformation continually induced into iPP.

The load curve of the second pass extrusion in route A [Fig. 2(b)] showed a double load peaks and obvious load drop after the maximum 11.6 kN, which is mainly due to the fact that some of the front region of specimens returned back when it flew into the horizontal channel. It was found that

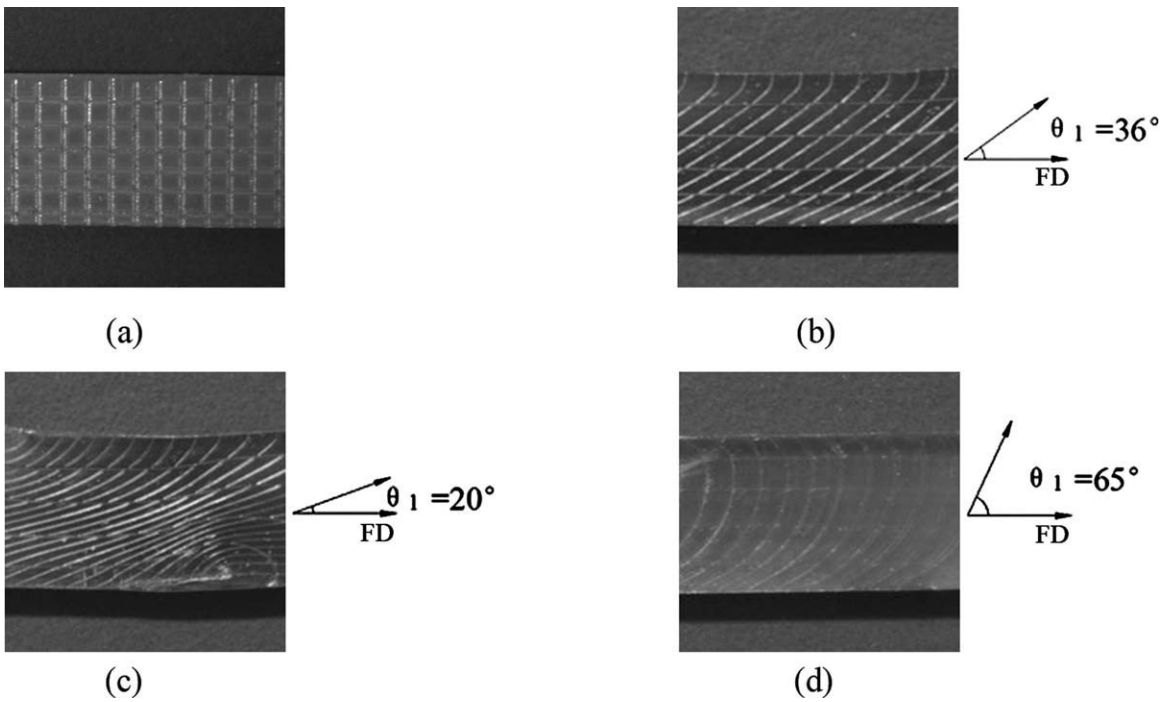

Figure 3 The grid on the FD-LD plane of (a) reference, (b) A1 sample, (c) A2 sample, (d) C2 sample. FD is to the right.

the required load was reduced for both the second pass extrusion in routes A and C. Such reduction was significant in route C [Fig. 2(c)], for example, the maximum load was 4.7 kN, which was 65% lower than that of A1 ECAE.

The macroscopic deformation of iPP samples was shown in Figure 3. To increase the visibility, the grid on the samples was coated by graphite before taking pictures. The deformation angle (θ_1) measured from FD to the tilted grid line (shear direction) is able to quantify the shear strain (γ) by using the formula $\gamma = \text{cotan}\ (\theta_1)$.[20,21] Under the present extrusion condition, the deformation angle θ_1 is about 36° in the central area of A1 sample, indicating that the induced shear strain (γ) is 1.38. The shear strain (γ) of A2 sample is progressively increased to 2.75, which will cause great change in the microstructure of iPP. If the sample is processed twice in route C, the total shear strain will be removed in theory, but complete cancellation of the total deformation was not observed in C2 sample with a residual shear strain of 0.47, which is likely due to nonzero-friction that occurred in practice.

Spherulitic morphology

Initially, the injection molded specimen often shows a hierarchical morphology through the thickness [named TD in Fig. 1(a)]. It has been reported that the injection molded iPP specimen is roughly separated into three layers along the thickness: a skin layer, a spherulitic core, and a "subskin" between these two layers.[22] The skin layer seems to be "structureless" due to a rapid cooling rate, which is difficult to be observed under ROM. Therefore, to investigate morphological changes processed by different ECAE routes, the FD-LD plane of the sample was polished carefully before etching to remove the outer surface. A literature[8] revealed the nature of ECAE deformation, which concluded that the shear deformation occurs only on the FD-LD plane, and the shear strain in TD is zero. That is why the present research of macroscopic deformation and spherulitic morphology was focused on the FD-LD plane of iPP samples by neglecting the variation along TD.

From the macroscopic observation of iPP samples, it was found that the shear strain was introduced to iPP by ECAE. As a consequence the plastic deformation of spherulites may occur in the ECAE-deformed iPP samples. The reflected optical micrographs were showed in Figure 4. The injection molded reference sample showed a typical spherulitic structure with long fibrous ribbons radiating out from a central point [Fig. 4(a)]. After one pass extrusion in route A, the original spherulites were deformed into nearly ellipsoidal shape with their long axis being inclined to FD [Fig. 4(b)]. The inclination angle (θ_2) measured between the long axis of the elliptical spherulite and FD was about 45° in A1 sample. After the second pass extrusion in route A, the spherulites appeared to be highly elongated with a small inclination angle of 30° [Fig. 4(c)]. The recovery of the spherulitic shape was exhibited in C2 sample [Fig. 4(d)]. As a consequence, the inclination angle obtained was 72°.

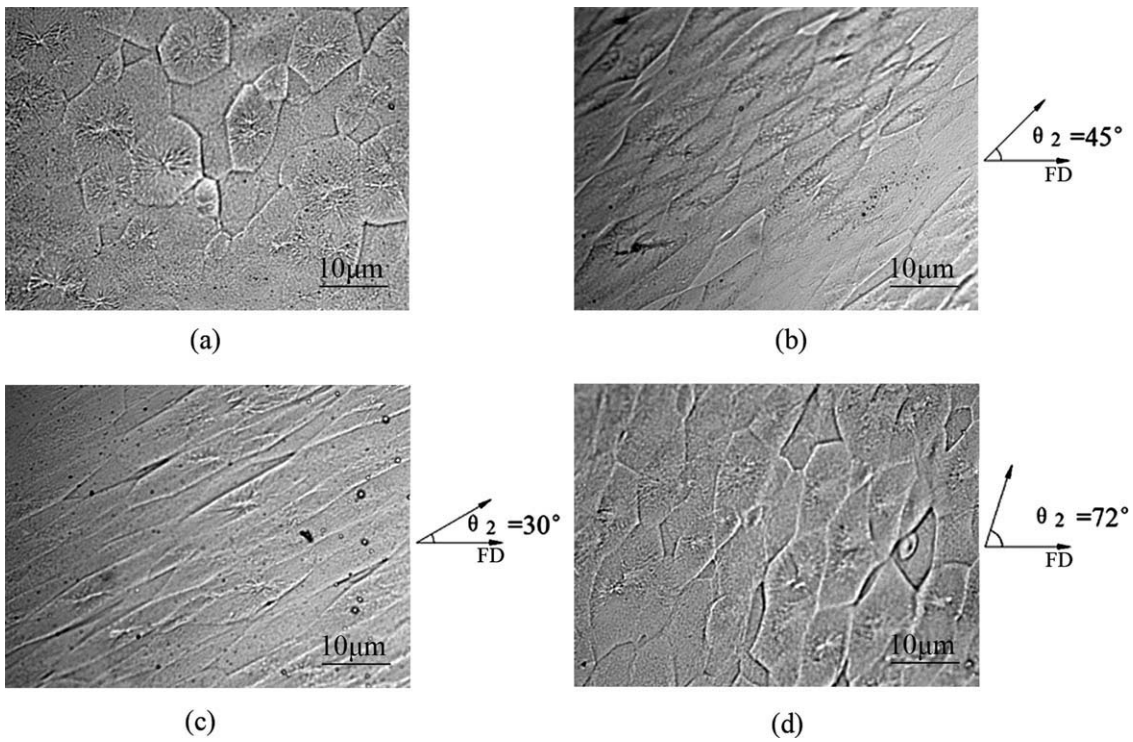

Figure 4 ROM of permanganate etched surface of (a) reference, (b) A1 sample, (c) A2 sample, and (d) C2 sample. FD is to the right.

During the optical observation of iPP samples, it was found that the plastic deformation is nonaffine at the spheulitic level. All spherulites can undergo large shear deformation; however, the comparison between inclination angle (θ_2) and the macroscopic deformation angle (θ_1) revealed that the spherulites deformed less than the overall specimen. Aboulfaraj et al.[23] observed the similar phenomenon. They explained this in terms of the complex morphology of monoclinic spherulites in polypropylene, where, the daughter lamellae interlocked with the parent lamellae,[24] resulting in structural resistance to deformation. X-ray and differential scanning calorimetry (DSC) measurements confirmed that the crystalline region in reference iPP sample is composed of monoclinic form. Therefore, the phenomenon that spherulites deformed less than the overall macroscopic deformation was also thought to be due to the interlocking nature of the parent-daughter structure stiffening them against the shear deformation.

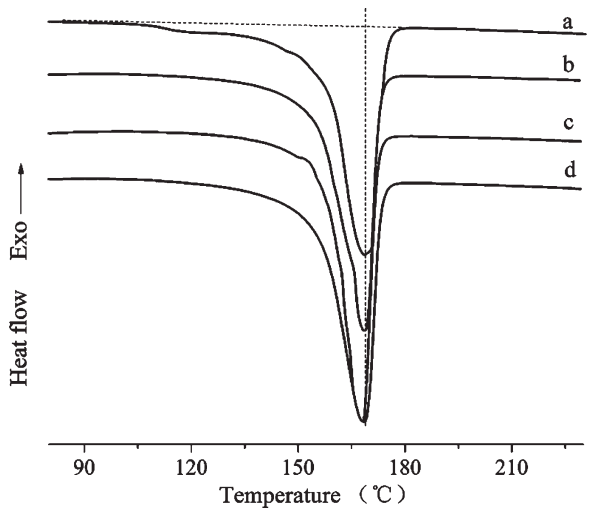

Figure 5 DSC curves of (a) reference, (b) A1 sample, (c) A2 sample, and (d) C2 sample.

Crystalline evolution of iPP

Large plastic deformation introduced by ECAE may change the crystallinity, the perfection of the crystals, and the orientation of both the crystalline and amorphous fraction of iPP samples. DSC method, density measurement, and X-ray diffraction were performed to evaluate the crystalline evolution of material. The results of DSC measurements on iPP samples are given in Figure 5 and Table I. The DSC curves indicated characteristic melting behavior of monoclinic crystals of iPP with the melting temperature T_m at the range of 167–169°C. It was also found that ECAE processing decreased the enthalpy of fusion ΔH, and eliminated a weak endothermic shoulder in the low temperature range with the onset at about 110°C. The X-ray diffraction intensity curves of iPP samples were shown in Figure 6, which confirmed the presence of monoclinic form in the studied samples.

TABLE I
DSC Results, Density, and the Crystallinity of iPP Samples

Sample	T_m (°C)	ΔH (J/g)	ρ(g cm^{-3})	X (%)		
				X_{DSC}[a]	X_V[b]	X_{XRD}[c]
Ref	168.6	105.4	0.9115	71.2	70.1	71.5
A1	168.7	98.0	0.9057	66.2	63.0	66.2
A2	167.5	94.7	0.9041	64.0	61.1	59.4
C2	168.6	100.8	0.9063	68.1	63.8	68.5

[a] The crystallinity calculated from ΔH.
[b] The crystallinity calculated from ρ
[c] The crystallinity calculated from the X-ray diffraction curves in Fig.6.

The density ρ and the crystallinity X estimated by ΔH, density and X-ray diffraction are collected in Table I. Although the estimates of crystallinity from different methods do not agree, the results suggested that ECAE processing disrupts the original structure of iPP and develops an altered structure with decreased crystallinity. A number of studies have described a decrease of crystallinity in semicrystalline polymers when subjected to large plastic deformation by uniaxial compression,[25] and plane-strain compression.[26,27] In these articles, it was reported that the crystallinity of compressed samples decreased with an increasing strain. Consistently, with the high shear strain, A2 sample results in a rapid decrease of crystallinity. The intense shear deformation can cause the lamellae fragment into small crystalline blocks, leading to crystalline orientation or amorphization of the system.

For quantitative evaluation of the X-ray diffraction curves in Figure 6, the separation of crystalline peaks from the amorphous halo was made by fitting the results through the software of MDI Jade 5.0. The corresponding crystalline peaks were analyzed in terms of the crystallite size L_{hkl} and the orientation parameter A_{110}. L_{hkl} was determined from the

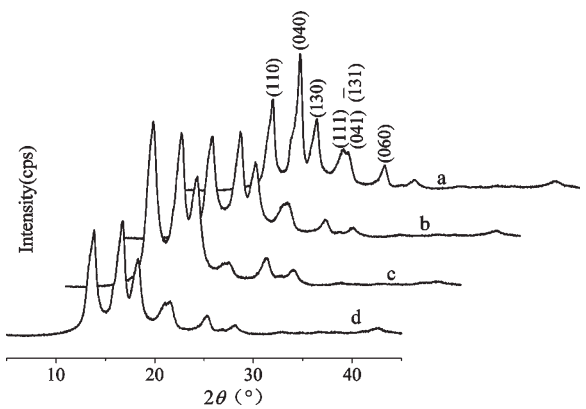

Figure 6 X-ray diffraction intensity curves of samples in 2θ scan: (a) reference, (b) A1 sample, (c) A2 sample, and (d) C2 sample.

TABLE II
The Calculated Results of iPP Samples from X-ray Diffraction Curves

Sample	L_{110} (nm)	L_{040} (nm)	L_{130} (nm)	A_{110}
Ref	9.6	15.6	10.6	0.617
A1	8.0	10.4	8.5	0.627
A2	7.5	8.9	8.2	0.810
C2	8.5	13.9	8.7	0.605

half-width of crystalline peak by applying Scherrer's equation.[28] Table II shows the comparison of L_{110} and L_{040} and L_{130} of iPP samples. The size reduction of the crystalline region was observed in the ECAE-deformed samples, which became pronounced in A2 sample.

Trotignon et al.[29,30] proposed a parameter A_{110} to evaluate the orientation of the crystalline region along the flow direction (FD). A_{110} is determined as:

$$A_{110} = \frac{I_{110}}{I_{110} + I_{111} + I_{\bar{1}31+041}} \quad (2)$$

The value of A_{110} depends on the vanishing (or decrease of intensity) of diffraction peaks of (111) and ($\bar{1}31$ + 041) in X-ray measurement. With respect to a highly oriented iPP crystallites, $A_{110} = 1$, otherwise $A_{110} < 1$. It was shown in Figure 6 that the peaks of (111) and ($\bar{1}31$ + 041) occurred in all samples, which indicated that in none of the samples do the orientation parameter A_{110} reaches the upper limit of 1. The calculated results in Table II showed that A2 sample has the highest A_{110}, 0.810, which indicates a preferential orientation along FD in A2 sample. The difference of A_{110} among other three samples was not pronounced, which may indicate that the crystallite orientation was not enhanced along FD during A1 or C2 ECAE procession. On the other hand, there exists a possibility that the crystallite orientation of A1 and C2 samples is along other direction different from FD.

Since the orientation parameter A_{110} can not reveal enough details of the orientation state of crystalline region in iPP samples, azimuthal scanning was performed to evaluate the crystal orientation. The (110), (040), and (130) crystallographic planes were selected for azimuthal scanning, and the X-ray patterns for the examined samples were sketched on the right side of the azimuthal scanning curves, see Figure 7.

The azimuthal distribution of the reference sample exhibited bimodal orientation from the (110) and (130) reflections, which is contributed both from the parent and daughter lamellae. Especially, the bimodal feature was easily identified from (110) reflection, where the parent section gave the meridional reflection and the daughter section gave the equatorial one.[31] The (040) reflection indicated that the

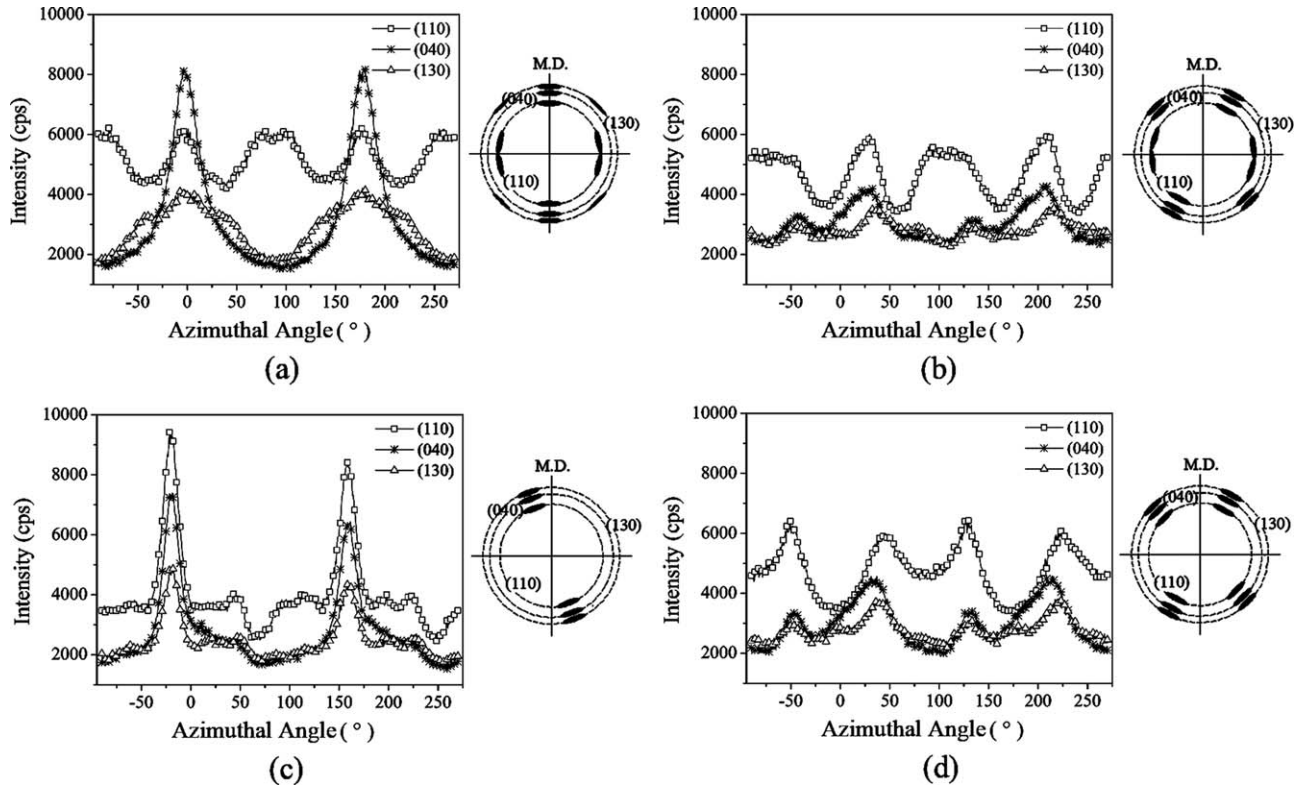

Figure 7 Azimuthal scanning curves of (110), (040), and (130) planes, and the X-ray patterns of (a) reference, (b) A1 sample, (c) A2 sample, and (d) C2 sample. FD is to the right.

crystallographic *b*-axis is preferentially perpendicular to FD. Although the apparent crystal orientation is presented in the reference sample because of the injection molding, the azimuthal distribution of this sample still indicated symmetrical reflections around the meridional or equatorial directions.

ECAE will induce different effects to iPP through mechanisms like interlamellar shear, crystallographic slips and associated crystal rotations.[32,33] It was found that the symmetrical reflections of crystallographic planes were not maintained in the azimuthal distribution of ECAE-deformed samples, which suggests that the rotation of crystals either by crystallographic slip or by rotation of lamellae takes place. After one pass extrusion in route A [Fig. 7(b)], the bimodal feature of the (110) plane remained but the maximum reflection of the daughter section was about 5° deviate from the equatorial direction. This small departure angle indicates that the daughter section rotate slowly than other crystalline sections. The reflection of the (040) and (130) plane split into two parts with their maxima at azimuthal angle about 28° clockwise and 45° anticlockwise to the meridional direction, as shown in Figure 7(b). This observed bimodal reflection of (040) and (130) plane can not be result from any parent-daughter effects, because similar bimodal distributions were observed in other polymer system which were not known to form parent-daughter structure, such as PET.[19] The bimodal feature of (040) and (130) reflections indicated the formation of two weak crystal orientation in A1 sample, one is 28°clockwise and the other is 45°anticlockwise to the meridional line. The angle of the orientation in our research appears to be different from that was found in iPP by Philips et al.[16] In their research, the isotropic reference samples were prepared by compression molding with limited molecular orientation. After one pass ECAE processing, two preferred orientation formed, one in the meridional position and the other inclined 27° anticlockwise to the meridional line. This indicates that the crystallographic planes rotate faster toward the shear direction then that in our experiment. A possible cause could be that the crystal orientation in our reference sample caused by injection molding will influence the crystalline evolution of iPP during ECAE.

As the iPP sample extruded twice in route A, the daughter lamellae lost their visibility, and more crystallographic planes rotated progressively toward the shear direction, resulting in a strong reinforcement of reflections around 20° anticlockwise to the meridional direction [Fig. 7(c)]. This suggested that the whole fold chain both of the parent section and the daughter section of iPP gradually merged and became one peak with the increased shear strain.

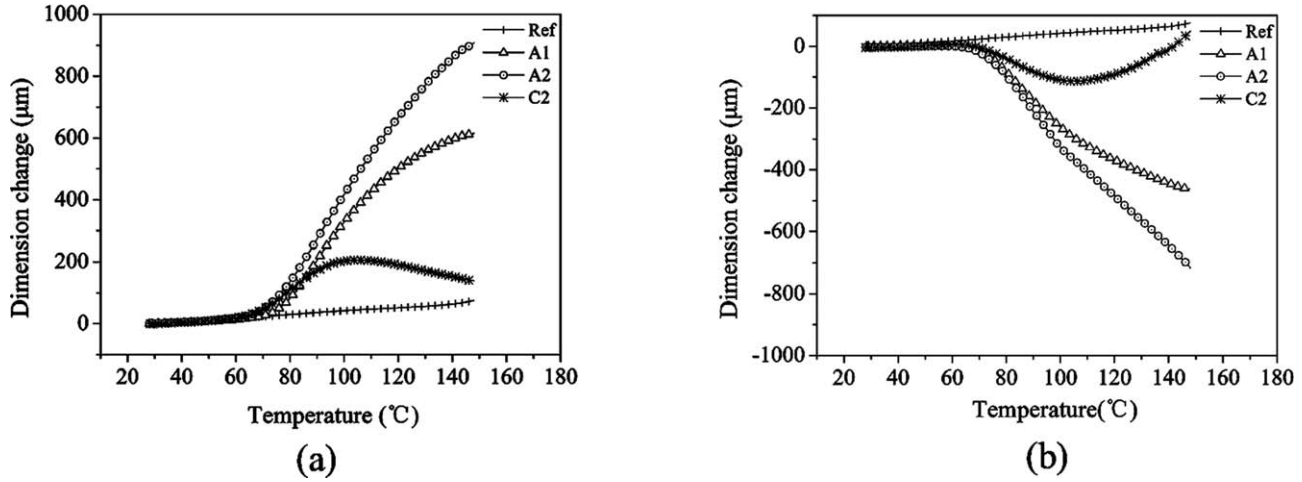

Figure 8 Dimension changes of iPP samples in the penetration mode DMA at (a) FD direction and (b) LD direction.

These new peaks appeared a relatively narrow azimuthal distribution, indicating the formation of high degree of crystal orientation in A2 sample. Philips et al.[16] ascribe these new reflecting peaks to the microfibrillar formation. From the azimuthal scanning curve of A2 sample, it was indicated that high shear strain can transform completely the initial orientation of the reference sample into microfibrils oriented along the shear direction.

Although the spherulitic deformation was almost removed in the second extrusion in route C, C2 sample demonstrated analogous set of peaks compared with those of A1 sample. The bimodal feature indicated that the crystal orientation was still reserved in C2 sample. But from the reflection of the (110) plane, it was seemed that the parent–daughter structure was probably destroyed in the second extrusion in route C.

Dynamic mechanical analysis

In the research of Xia et al.,[19] the annealing test was performed between the glass transition temperature (T_g) and the melting point (T_m) to examine the ECAE-induced deformation in the amorphous region of PET. The principle is that the original shape of the PET sample will be partially recovered owing to the relaxation of the amorphous region. Different from the annealing test which took photographs to reflect the recovery of shape, penetration mode DMA performed at FD and LD directions is able to quantitatively record the dimension changes of iPP samples.

It was shown in Figure 8 that the thermal expansion of reference sample increased linearly with the temperature increasing, but the total amount of expansion was slight because the relaxation of the amorphous domains were bounded by the crystalline regions. The dimension changes of ECAE-deformed samples were similar to that of the reference sample until the ECAE processing temperature 65°C was approached. Above 65°C, the relaxation of amorphous phase in the ECAE-deformed samples took place leading to distinctive thermal contraction at FD direction, and thermal expansion at LD direction. The thermal contraction/expansion behavior of A2 sample was similar to that of the A1 sample owing to the same processing route. The maximum dimension change indicated the largest deformation of the amorphous region in A2 sample. The dimensional change of C2 sample was less than that of A1 sample, which meant that the deformation of the amorphous region was already partially recovered in route C. It also found that the relaxation of amorphous region was exhausted when the temperature was above 100°C, and the contraction/expansion behavior of C2 sample was suppressed again by the adjacent crystalline region.

Consequently, we concluded that the dimensional change in the penetration mode DMA was due to the ECAE process. The contraction/expansion behavior of ECAE-deformed samples indicated that the long chain molecules in amorphous region were stretched at FD direction, and were compressed at LD direction after ECAE process, which will result in the modification of the mechanical response of the ECAE-deformed samples.

The storage modulus (E') and loss tangent (tan δ) were shown in Figure 9. The microstructure changes resulted from ECAE process are responsible for the difference in dynamic mechanical behavior of iPP samples. The distinctive trend for E' is $E'_{A2} > E'_{A1} > E'_{Ref} > E'_{C2}$ in the temperature range of −50°C to T_g (roughly 14°C, where there is a β-relaxation in the reference sample). At temperature below T_g, the response of iPP sample in DMA was dominated by the amorphous region. Such a specific response of iPP samples extruded in route A most probably

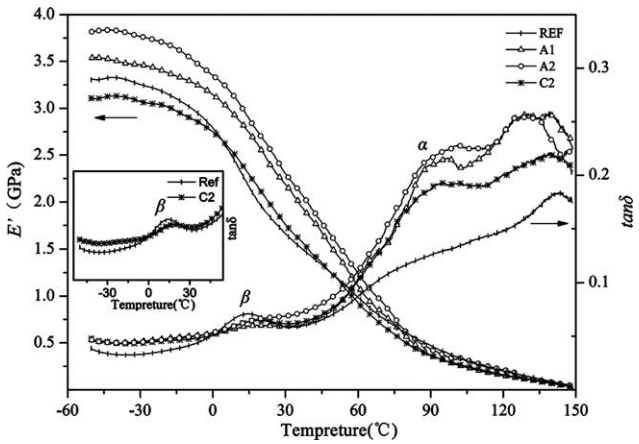

Figure 9 Storage modulus (E') and loss tangent (tan δ) of iPP samples based on dual cantilever mode DMA (inset: the β-relaxation peak of the reference and C2 samples).

resulted from the strong constraint imposed by the slip deformation in the crystalline region to which the amorphous region is intimately connected. And A2 sample becomes stiffer than other samples due to the higher strained molecules in amorphous region. The β-relaxation peak in the tan δ curve (Fig. 9) was almost disappeared in A1 and A2 samples. It is known that the β-relaxation is associated with glass-rubber transition of the amorphous phase of iPP.[34] The disappearance of the β-relaxation peak implied clearly a substantial reduction of mobility of chains in the amorphous region in A1 and A2 samples. As for C2 sample, the deformation recovery and the destruction of parent–daughter structure may result in weaker constrains imposed on the amorphous region. Therefore, the β-relaxation peak of the tan δ curves reappeared in C2 sample (shown by the inset in Fig. 9), but with a reduced intensity.

Above T_g, the amorphous phase will become soft. Most of the resistance to the testing deformation results from crystalline phase in iPP samples. The values of E' at selected temperature were presented in Table III. A2 sample still has the highest E' in the temperature range T_g −80°C as compared with other samples, which was contributed to the highly oriented crystalline in A2 sample. The α-relaxation

TABLE III
The Storage Modulus (E') of iPP Samples at Different Temperature Above T_g

	E' (GPa)				
Sample	30 (°C)	60 (°C)	80 (°C)	90 (°C)	100 (°C)
Ref	1.66	0.99	0.60	0.47	0.36
A1	2.19	1.10	0.56	0.36	0.27
A2	2.30	1.24	0.62	0.43	0.33
C2	1.75	0.93	0.49	0.36	0.28

appeared as a shoulder at about 90°C indicated on tan δ curves (Fig. 9). It was found that the α-relaxation is facilitated in ECAE-deformed samples, which may come from the decrease of crystallinity of these samples.

Optical property

After ECAE, iPP samples became translucent. As shown in Figure 10, the printed letters are clearly visible through A1 sample in contrast to the reference sample. The results in Figure 11 showed that the luminous transmittance of the ECAE-deformed samples is increased comparing with that of the reference sample. Furthermore, A2 sample with high shear deformation showed the highest luminous transmittance in iPP samples. Worth noticing is that Bartczak et al.[35] observed the similar phenomenon that the rolled iPP with the higher deformation ratios become more transparent in contrast to the opaque bar of neat iPP.

In the case of semicrystalline polymers, light scattered on the different structure units will make the products opaque.[36] In iPP sample, the incident light is scattered on the spherulites, crystllites, and also on the interface between the amorphous and crystalline phases having different refractive indices. The incident light wavelength is ranged from 380 to750 nm. Often the spherulites are large enough to interfere with the incident light and this interference results in the loss of transparence.[37] Therefore, the shear destruction of spherulites induced by ECAE will increase the luminous transmittance of iPP. In

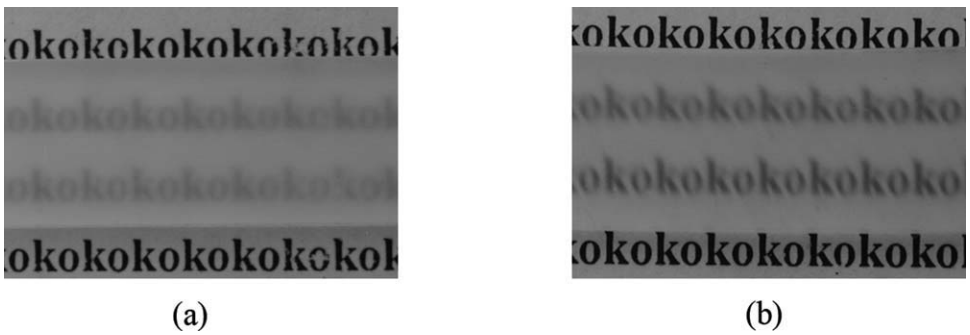

Figure 10 The photographs of (a) reference and (b) A1 sample.

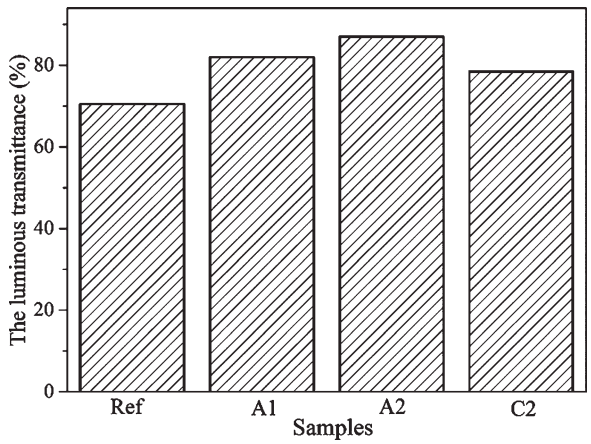

Figure 11 Luminous transmittance results of iPP samples.

addition, the crystalline structure change such as crystalline size reduction and crystal orientation initially organized in a higher order spherulitic morphology is also benefit for the increasing of transparency with reduced refractive index fluctuations.

Izod impact testing results

Neat iPP is always comparatively brittle due to its monoclinic spherulites that has been formed under normal crystallization conditions, thus limiting its applications. A widely employed strategy for improving the impact strength of iPP has involved in the incorporation of dispersed elastomeric[38] or rigid phase.[39] Different from the addition of the second phase to the polypropylene matrix, iPP has an opportunity to be self-reinforced by solid state orientation. As discussed in the previous paragraphs, ECAE process has been shown to be effective in orienting iPP material. The notched Izod impact testing was achieved to highlight the orientation structure on the impact fracture behavior of ECAE-deformed iPP samples.

The crack development of iPP samples after Izod impact test was shown in Figure 12. The reference sample showed a normal crack paralleling to the impact direction, however, the crack of the ECAE-deformed samples was different and spread out along the shear direction similarly. Furthermore, the inclination angle θ_3 between the crack and FD (shown in Fig. 12) was consistent with the spherulites deformation angle θ_2 (Fig. 4). Previous observations of crack initiation and propagation through centers and boundaries of spherulites indicate that these are sites of weakness in spherulites of iPP, often resulting in premature mechanical failure.[40–44] According to this view, the inclination of the crack further confirms the deformation of spherulites in ECAE-deformed samples.

The notched Izod impact strength of iPP samples was compared in Figure 13. After one pass extrusion in route A, the impact strength of iPP was increased

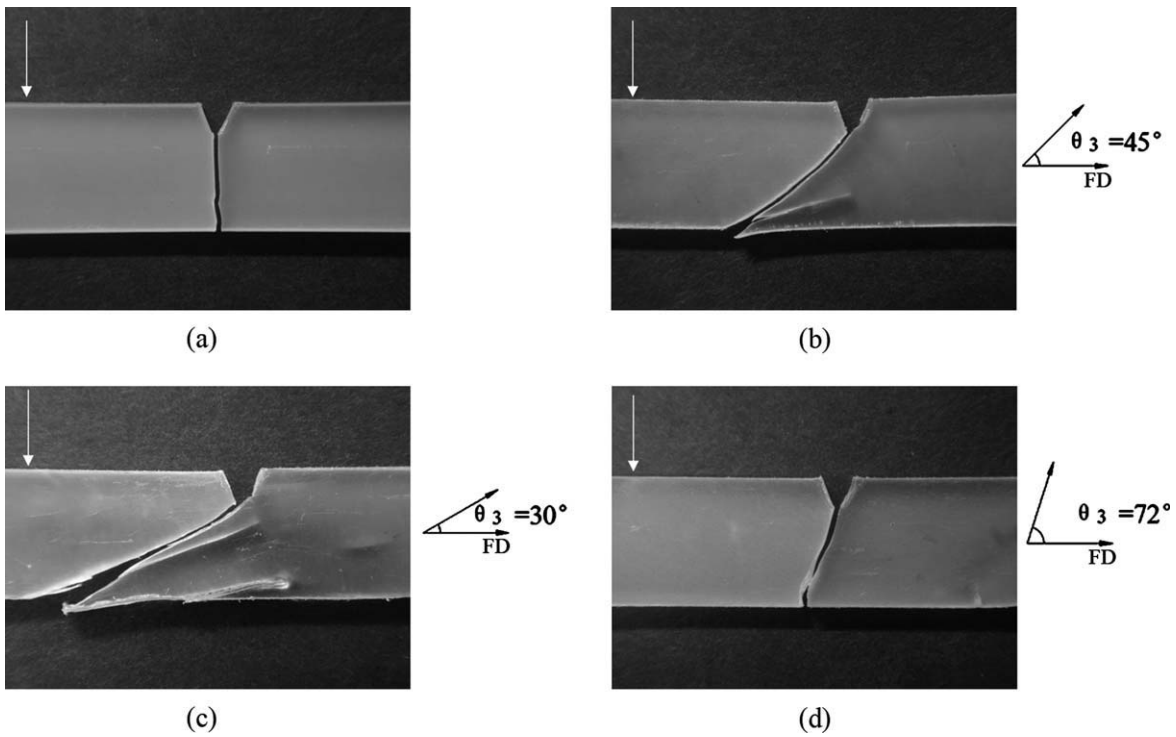

Figure 12 Photographs of iPP samples after Izod impact testing: (a) reference, (b) A1 sample, (c) A2 sample, and (d) C2 sample. The white arrows indicate the impact direction. FD is to the right.

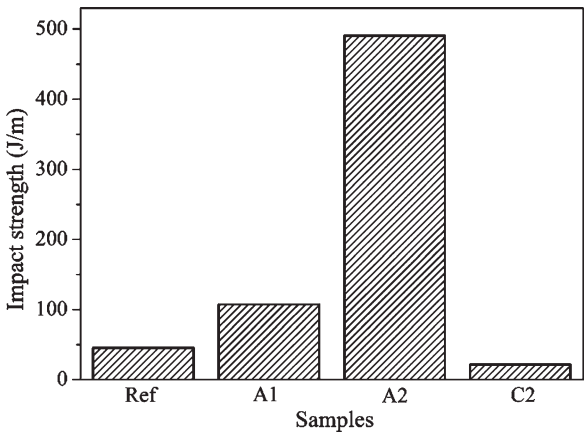

Figure 13 The Izod impact strength of iPP samples.

to 107.2 J/m. Moreover, the impact strength of A2 sample was greatly improved and reached 490.5 J/m, which is 10 times to that of the reference sample (45.3 J/m). However, less fracture resistance was encountered in C2 sample and showed only 52% of the impact strength of the reference sample.

Considering iPP samples extruded in route A, one realized that they exhibits higher resistance toward Izod impact crack propagation than the reference sample. One explanation influencing impact resistance is the microstructure orientation during ECAE. Since 1960s, several models[45–47] have been proposed to understand the structure-property relationship in oriented semicrystalline polymers. Among these models, the fibril model first proposed by Peterlin[46] has been proved to be successful in understanding Young's modulus increase in along FD in ECAE-oriented PET sample.[9] The key feature of fibril model is the formation of the macro- or microfibrillar structures. The macrofibrils are transformed from the original spherulites, while the microfibrls are originated from the initial crystalline lamellae. As a result, two types of taut tie molecules (TTMs) will be found: intermacrofibrillar and intemicrofibrillar TTMs. The experiment results mentioned above indicated that the original spherulites have been highly elongated into macrofibrils after ECAE. These macrofibrils will render the material more resistant to crack development and deflect the direction of the primary crack to propagate at an angle with FD. Moreover, to accommodate the orientation of fibril structure, it is highly likely that the TTMs connecting these fibrils become stretched along FD in the iPP samples extruded by route A. One proof is that A1 and A2 samples showed distinctive thermal contraction at FD direction in the penetration mode dynamic mechanical analysis. When these highly stretched molecular is perpendicular to the impact direction, more energy to be required for the crack

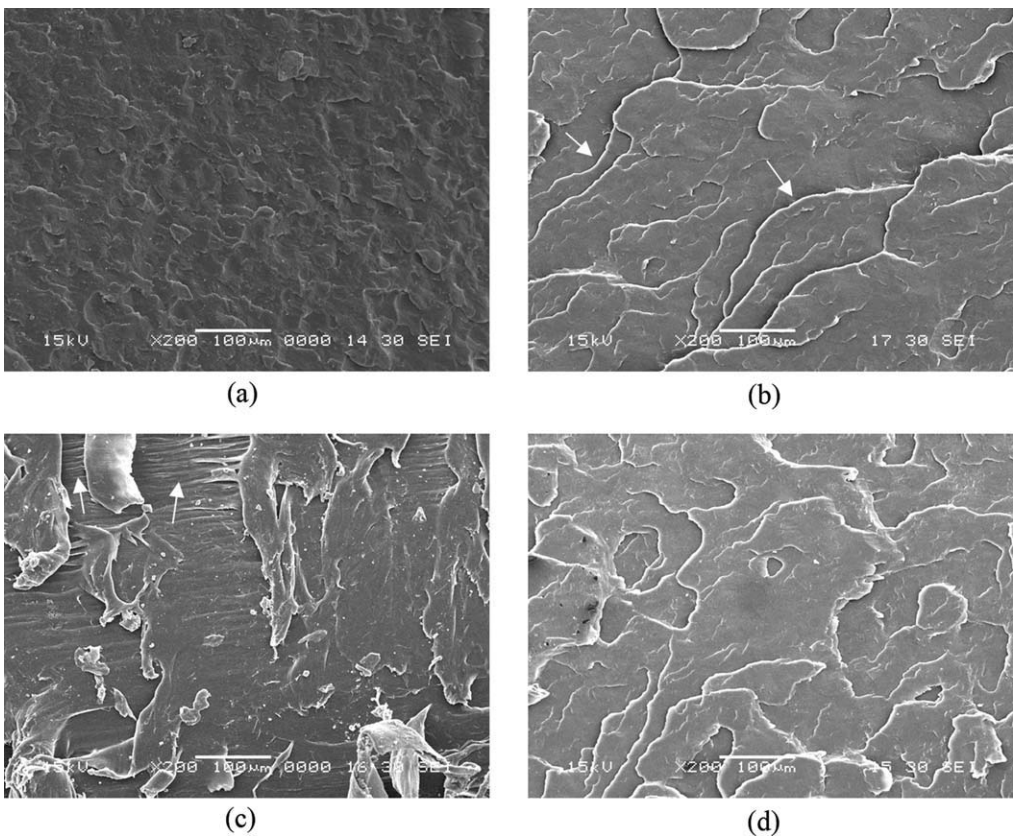

Figure 14 SEM micrographs of the impact fractured surface of (a) reference and (b) A1 sample.

propagation. It had been found that two pass extrusions in route A resulted in a finer fibril structure than one pass. In the case of A2 sample the initial structure was transformed completely into microfibils as observed by azimuthal scanning. Furthermore, the fraction of intermicrofibrillar TTMs in A2 sample will be increased by the chain unfolding in the microfibrils formation. These TTMs will also improve interlamellar adhesion, resulting in highest improved impact strength for A2 sample. Although there is no clear explanation for the decrease of the impact strength of C2 sample, the following suggestion can be raised. The microcracks/crazes formed by microdomain rotation in C2 ECAE processing may have a deleterious effect on the Izod impact properties of C2 sample. These pre-existed microcracks/crazes were not investigated in my research, but were observed in C2 ECAE processed PET.[9]

The impact fractured surface was examined in Figure 14 to understand further the nature of the deformation mechanism involved during crack propagation. The fracture surface of reference sample appeared flat and smooth. Wave-like break lines [indicated by the arrows in Fig. 14(b)] were found in A1 sample. Whereas, C2 sample showed irregular break lines in contrast to A1 sample. These fracture features may relate to the point that the spherulites centers or boundaries accommodate high stress concentrations and develop crazing and cracking preferentially under deformation.[41,44] Spherultic morphology changes may result in different appearances of break lines for A1 and C2 samples. On the other hand, a very rough texture involving fibrous zones [indicated by the arrows in Fig. 14(c)] was observed in the fracture surface of A2 sample. Different from the crazing deformation mechanism in other samples, this feature indicated that plastic deformation in front of the crack tip must have occurred during crack propagation. A possible explanation for this change is the formation of microfibrillar structures with TTMs in A2 sample, which alter the stress state in the material and induce plastic deformation with considerable energy dissipation.

CONCLUSION

ECAE is a potential technique to manipulate the morphology of polymer in solid state. iPP was processed for up to two passes in routes A and C at 65°C by ECAE. It was shown that high shear strain about 2.75 is introduced to iPP extruded twice in route A. Morphological evolution induced by processing routes in ECAE was measured by ROM and X-ray diffractions. The spherulites of iPP appeared to be elongated into ellipsoidal shape and oriented along the shear direction in route A, and the recovery of the spherulitic shape exhibited in iPP sample extruded in route C. ECAE processing decreased the crystallinity, as estimated from DSC, density and X-ray diffraction; it thus disrupts the original structure of iPP, developing an oriented crystalline structure. The azimuthal scanning suggested that the crystal rotation took place by the shear deformation, resulting in two weak crystal orientations in A1 sample and a high degree of crystal orientation A2 sample. The penetration mode DMA confirmed that the amorphous phase of iPP is highly strained in route A, which is responsible for the increase of the high dynamic storage modulus (E'). After processed in routes A and C, iPP sample exhibited different Izod impact behavior. The ECAE-deformed spherulites play a dominant role in the crack propagation direction. The inclination angle of the crack is consistent with the spherulites deformation angle. iPP samples extruded in route A exhibited higher notched Izod impact strength than the un-deformed reference sample, especially, the impact strength of A2 sample was greatly improved due to the oriented structure. However, less fracture resistance was encountered in iPP sample extruded in route C.

The authors thank Professor Yuping Zhu (Donghua University) for his help with X-ray characterization. Dr. Shengguang Weng (East China University of Science and Technology) is also gratefully acknowledged for his help with dynamic mechanical analysis.

References

1. Segal, V. M.; Reznikov, V. I.; Drobyshevkiy, A. E.; Kopylov, V. I. Russ Metal 1981, 1, 99.
2. Mohanraj, J.; Chapleau, N.; Ajji, A.; Duckett, R. A.; Ward, I. M. Polym Eng Sci 2003, 43, 1317.
3. Ariyama, T. J Mater Sci 1996, 31, 3813.
4. Lezak, E.; Bartczak, Z. J Polym Sci Poly Phys 2008, 46, 92.
5. Bartczak, Z.; Morawiec, J.; Galeski, A. J Appl Polym Sci 2002, 86, 1413.
6. Segal, V. M. Mater Sci Eng A 1999, 271, 322.
7. Sue, H. J.; Li, C. K. Y. J Mater Sci Lett 1998, 17, 853.
8. Campbell, B.; Edward, G. Plast Rubber Compos 1999, 28, 467.
9. Xia, Z. Y.; Hartwig, T.; Sue, H. J. J Macromol Sci Phys 2004, 43, 385.
10. Li, C. K. Y.; Xia, Z. Y.; Sue, H. J Polymer 2000, 41, 6285.
11. Xia, Z. Y.; Sue, H. J.; Hsieh, A. J. J Appl Polym Sci 2001, 79, 2060.
12. Weon, J. I.; Creasy, T. S.; Sue, H. J Polym Eng Sci 2005, 45, 314.
13. Creasy, T. S.; Kang, Y. S. J Mater Process Tech 2005, 160, 90.
14. Weon, J. I.; Sue, H. J Polymer 2005, 46, 6325.
15. Sue, H. J.; Dilan, H.; Li, C. K. Y. Polym Eng Sci 1999, 39, 2505.
16. Phillips, A.; Zhu, P. W.; Edward, G. Macromolecules 2006, 39, 5796.
17. Olley, R. H.; Bassett, D. C. Polymer 1982, 23, 1707.
18. Viana, J. C.; Cunha, A. M.; Billon, N. Polymer 2002, 43, 4185.
19. Xia, Z. Y.; Sue, H. J Macromolecules 2000, 33, 8746.
20. Segal, V. M.; Hartwig, K. T.; Goforth, R. E. Mater Sci Eng A Struct 1997, 224, 107.
21. Baker, I.; Wu, Y. Scripta Mater 1997, 37, 43.

22. Yu, X. F.; Wu, H.; Li, J.; Guo, S. Y, Qiu, J. H. Polym Eng Sci 2009, 49, 703.
23. Aboulfaraj, M.; G'sell, C.; Ulrich, B.; Dahoun, A. Polymer 1995, 36, 731.
24. Lotz, B.; Wittmann, C. J. J Polym Sci Poly Phys 1986, 24, 1541.
25. Bartczak, Z.; Cohen, R. E.; Argon, A. S. Macromolecules 1992, 25, 4692.
26. Lima, M. F. S.; Vasconcellos, M. A. Z.; Samios, D. J Polym Sci Polym Phys 2002, 40, 896.
27. Pluta, M.; Bartczak, Z.; Galeski, A. Polymer 2000, 41, 2271.
28. Alexander, L. E. X-ray Diffraction Methods in Polymer Science; Wiley: New York, 1979.
29. Trotignon, J. P.; Lebrun, J. L.; Verdu, J. Plast Rubber Process Appl 1982, 2, 247.
30. Trotignon, J. P.; Verdu, J. J Appl Polym Sci 1987, 34, 1.
31. Zhu, P.W.; Edward, G. J Mater Sci 2008, 43, 6459.
32. Galeski, A.; Bartczak, Z.; Argon, A. S.; Cohen, R. E. Macromolecules 1992, 25, 5705.
33. Lin, L.; Argon, A. S. J Mater Sci 1994, 29, 294.
34. Lee, S. H.; Kim, S. Y.; Youn, J. R. Composites Part A Appl Sci 2009, 40, 968.
35. Bartczak, Z.; Morawiec, J.; Galeski, A. J Appl Polym Sci 2002, 86, 1413.
36. Stein, R. S.; Rhodes, M. B. J Appl Phys 1960, 31, 1873.
37. Qamer, Z.; René, A.; Hans, J. R. J Appl Polym Sci 2010, 117, 1013.
38. Jafari, S. H.; Gupta, A. K. J Appl Polym Sci 2000, 78, 962.
39. Thio, Y. S.; Argon, A. S.; Cohen, R. E. Polymer 2004, 45, 3139.
40. Lustiger, A.; Marzinsky, C. N.; Mueller, R. R. J Polym Sci Polym Phys 1998, 36, 2047.
41. Friedrich, K. Prog Colloid Polym Sci 1978, 64, 103.
42. Way, J. L.; Atkinson, J. R.; Nutting, J. J Mater Sci 1974, 9, 293.
43. Nitta, K. H.; Takayanagi, M. J Mater Sci 2003, 38, 4889.
44. Wei, G. X.; Sue, H. J.; Chu, J.; Huang, C. Y.; Gong, K. C. J Mater Sci 2000, 35, 555.
45. Peterlin, A. J Mater Sci 1971, 6, 490.
46. Ward, I. M. J Polym Sci Polym Symp 1973, 32, 195.
47. Nitta, K. H.; Takayanagi, M. J Polym Sci Polym Phys 1999, 37, 357.